An unsteady wake-source model for flow past an oscillating circular cylinder and its implications for Morison's equation

By Y. T. CHEW, H. T. LOW, S. C. WONG AND K. T. TAN

Department of Mechanical and Production Engineering, National University of Singapore, 10 Kent Ridge Crescent, Singapore 0511

A potential-flow modelling of flow past an oscillating circular cylinder with separated wake is developed here based on Parkinson & Jandali's (1970) wake-source model for steady flow. The phase-averaged pressure distributions, the in-line force coefficients, as well as the drag and added-mass coefficients, for an in-line oscillating circular cylinder in a steady free-stream flow are computed using the present 'unsteady wake-source model'. The results show that Morison's equation is in some cases a satisfactory model in the study of unsteady bluff-body aerodynamics.

The two-dimensional incompressible potential-flow model simulates the effect of flow separation in unsteady flow by placing surface sources, with time-dependent strength and angular positions on the rear wetted surface of the body, and downstream sinks to form a closed wake model in the transformed plane. The unsteady Bernoulli equation is used to obtain the time-dependent pressure distributions over the front wetted surface, from which the in-line force coefficients are obtained through integration.

The in-line force equation obtained from the present model is shown to be comprised of an uncoupled drag term and inertia terms. The corresponding hydrodynamic coefficients obtained for the case of oscillatory flow are also more realistic than those obtained in a potential-flow calculation without flow separation which gives a drag coefficient of zero and a constant inertia coefficient of 2.0. The in-line force equation is reduced to the familiar Morison's equation with some simplifications and thus provides some support to the much criticized Morison's equation in the study of unsteady separated flow.

Another interesting feature of the present model is that it enables the calculation of instantaneous drag and inertia coefficients which have not been successfully obtained previously. In the cases considered here, the variations of drag and inertia coefficients over a cycle are shown to be small and thus the Morison's equation using mean coefficients is shown to predict the in-line forces rather precisely.

The present model was compared with experimental measurements obtained by oscillating a 0.1 m diameter circular cylinder along the direction of free-stream flow. The pressure distributions and in-line force coefficients agree well with the experimental measurements for velocity ratio $r\omega/U_\infty$ up to 0.25, reduced velocity $U_\infty T/d$ down to 50 and Keulegan–Carpenter number $2\pi r/d$ up to 17, where r, ω, T, U_∞ and d are the amplitude of oscillation, angular frequency, period of oscillation, free-stream velocity and diameter of the cylinder respectively. The computed drag and inertia coefficients also agree well with those obtained experimentally by previous investigators.

1. Introduction

The understanding of unsteady flow past a stationary bluff body, or an oscillating body in a mean flow, has important applications in the design and study of offshore and coastal structures, ocean pipelines and risers. When an engineering structure is being towed or sited in an ocean environment, the flow field around the structure generally consists of a superimposed oscillatory wave and a mean flow. At high Reynolds numbers, the resulting flow consists of a separated wake with vorticity being shed continually from the separation locations. In this flow regime, the vortex-flow force which corresponds to the form drag becomes comparable with, or even larger than, the inertia force and the viscous force is insignificant. An irrotational flow wave-load calculation which ignores the effect of flow separation is incorrect since the physics of the flow is not appropriately represented.

To date, there is no complete theory or modelling available to predict the flow behaviour for such a flow because of the complexity of bluff-body aerodynamics at very high Reynolds numbers. Free-streamline models have been applied to steady potential flow in which the velocity, pressure distribution around the cylinder and separation locations are considered as two-dimensional time-averaged quantities. In these solutions, which separate the irrotational external flow from the rotational wake region, the wake region is not amenable to potential flow calculation, but its effect in the form of wake pressure must be obtained from experiment as an empirical input to the potential flow calculation. For a smooth-surface body-like circular cylinder where the size of the wake region is not well defined, additional empirical input on separation locations must also be specified. The shapes of the separation free streamlines are initially unknown, but the velocity distributions along them can be specified. These, together with the usual inviscid boundary condition on the body surface upstream of separation locations, enable the solution of the irrotational flow region using conformal transformation techniques to be found. Examples of these theoretical methods are the free streamline theories developed by Roshko (1954), Woods (1955) and Wu (1962), which show good agreement between the measured and predicted time-averaged surface pressure on simple two-dimensional bluff bodies. These methods were further refined by Parkinson & Jandali (1970) who specified the free-streamline positions using two wake-sources and their cor-responding images in the complex transformed plane. The strength and positions of wake-sources are found by satisfying the specified separation locations and pressure in the complex plane. The solution of the flow field in the complex plane is then transformed to that past a slit corresponding to the wetted surface of the body in the physical plane. The transformation is chosen such that the free-streamlines and stagnation points in the complex plane correspond to the separation shear layers and separation locations in the physical plane, with the added condition that the physical flow leaves the body surface tangentially at the separation locations. The physical flow field between the separation streamlines in the wake region is ignored. The prediction accuracy of their method is comparable to the other free-streamline theories, but it has the advantage of being simpler to apply.

Bearman & Fackrell (1975) incorporated some of the ideas underlying the wake-source method of Parkinson & Jandali, but without using conformal transformation so their method can be used for calculating potential flow about bluff bodies of arbitrary shape. They use a distribution of discrete vortices to represent the wetted surface of the body and the solution is obtained by numerical methods. Their results on the pressure distributions agree well with that obtained from the analytic

expressions by Parkinson & Jandali. Kiya & Arie (1977) also incorporated some of the ideas underlying Parkinson & Jandali's wake-source model by taking into account the displacement effect of the far-wake by means of a source–sink system located behind the body. In this way, the far-wake displacement effect, causing wind-tunnel blockage, is properly deduced. Celik, Patel & Landweber (1985) proposed a boundary-layer calculation method which computes the separation locations and displacement thickness. These are then taken into account in the irrotational-flow model to compute the pressure distribution needed in the boundary-layer calculation. The iterative calculation procedure which represents the viscous–inviscid interaction continues until convergence occurs. Their method can predict the locations of separation, drag coefficient, and pressure-distribution parameters at Reynolds number as high as 10^8.

In spite of the interest in unsteady flow past a bluff body and many experimental measurements of the unsteady-flow-induced forces, there are few numerical works in this area because of its complexity. Analytical solution of separated time-dependent flow is not yet possible even for relatively idealized situations. Hurlbut, Spaulding & White (1982) presented a finite difference model for viscous two-dimensional flow of a uniform stream past an oscillating cylinder. A non-inertial coordinate trans-formation is used so that the grid mesh remains fixed relative to the accelerating cylinder. Three types of cylinder motions are considered: oscillation in a still fluid, oscillation parallel to a moving stream and oscillation transverse to a moving stream. The results were computed for cases when the cylinder oscillation is near the natural vortex-shedding frequency. However, the method is limited to Reynolds number lower than 100. Lecointe & Piquet (1989) presented a numerical solution of the unsteady two-dimensional Navier–Stokes equations using an ADI Peaceman–Rachford time discretization and a fourth-order accurate OCI spatial scheme for flow of Reynolds number up to 855. They investigated the vortex-shedding characteristics behind a circular cylinder immersed in a uniform stream and performing superimposed in-line and transversed oscillations. Harmonic, sub-harmonic and superharmonic excitations were considered and their results compared favourably with experimental measurements. Finite-difference simulations of unsteady flow about stationary and oscillating cylinders have also been carried out by Tamura, Tsuboi & Kuwahara (1988). There have also been some numerical studies on zero-mean oscillating flow around circular cylinders. Justesen (1991) and Baba & Miyata (1987) carried out studies based on finite-difference analysis of the Navier–Stokes equation. Vortex methods have also been used by Smith & Stansby (1991), Skomedal, Vada & Sortland (1989) and Mostafa (1987) to study such flow.

The present study is undertaken with the following two objectives in mind. The first objective is to derive, from potential-flow consideration, a theoretical or semi-theoretical model for the prediction of pressure distributions and hence the in-line forces for an along-flow oscillating cylinder in a mean flow. The second objective is to examine the possibility of deducing the widely used Morison's equation from the present model. The real unsteady separated flow is approximated by the following assumptions based on some empirical observations.

(i) The experiment flow field which provides the empirical inputs, though unsteady, is uniform and the time phase-averaged quantities, such as velocity and pressure distribution, are reasonably two-dimensional except near the ends of the body-span.

(ii) The boundary layer and the separation shear layer are assumed thin and well-

defined close to the body, and the flow field is irrotational everywhere external to the boundary layer and shear layer.

(iii) The free-steam flow velocity is assumed to be sufficiently high to convect the shed vortices downstream such that there is negligible direct interaction between the vortices and the cylinder during the in-line oscillation, and the oscillation frequency does not interact with the vortex-shedding frequencies.

(iv) The separation locations are assumed to be constant during each cycle of oscillation as a corollary of assumption (iii).

(v) It is experimentally observed (as shown in figures 4–6) that the phase-averaged back pressure over the body surface exposed to the wake is approximately uniform and its value is close to that at the separation locations. Therefore, in the modelling, the phase-averaged separation pressure is assumed to be equal to the phase-averaged back pressure averaged over the body surface exposed to the wake.

These assumptions point out the possibility of extending Parkinson & Jandali's model to unsteady flow by incorporating the time-dependent wake-sources of varying strength and angular positions to account for the time-dependent separation velocity. The empirical inputs are the separation locations, which are assumed fixed, as stated in assumption (iv), and the time-dependent phase-averaged wake pressure. The unsteady Bernoulli equation is used to determine the unsteady pressure distribution. A preliminary attempt based on an open wake, as in the Parkinson & Jandali's (1970) original steady flow wake-source model, was abandoned owing to the problem of infinite unsteady potential in the far field, which is induced by the unbound pulsating sources. In the present model, the wake is closed, and the conformal mapping and Bernoulli equation are applied directly to a non-inertial frame of reference which is attached to the centre of the oscillating cylinder (Milne-Thomson 1968, pp. 87–103).

2. The unsteady wake-source model

The physical and transformed planes of the unsteady wake-source model for a two-dimensional, incompressible and irrotational unsteady flow past a bluff body are shown in figure 1. The physical flow consists of a circular cylinder with oscillating velocity $-U(t)$ being placed in a uniform free-stream flow U_∞ in the direction of the real axis. The flow is symmetrical about the horizontal plane with two separation locations at S_1 and S_2 respectively. In the physical Z-plane, part of the physical surface S_1AS_2 is mapped conformally from the corresponding part of the circle γ in the ζ-plane by the analytic function

$$Z = f(\zeta). \tag{1}$$

It should be noted that, since the circle γ is also oscillating, the transformation is applied with respect to the body-centred (non-inertial) frame of reference.

The transformation preserves the direction, but not necessarily the magnitude, of the incident flow as seen in the moving frame. With the wake region in the physical Z-plane being ignored, the physical slit $S_1AS_2BS_1$ in the Z-plane is mapped from the complete circle γ of radius R in the ζ-plane.

In the complex ζ-plane as shown in figure 1(b), the flow field past the oscillating circle γ, with oscillating velocity $-V(t)$, is comprised of a uniform steady free-stream flow V_∞ past a suitable doublet. Sources, of strength $2Q(t)$ each, are symmetrically located at the time-dependent source angles $\pm\delta(t)$ on the arc S_2BS_1 of circle γ. A double-sink of strength $-2Q(t)$ is placed along the real axis at location $(mR, 0)$, where
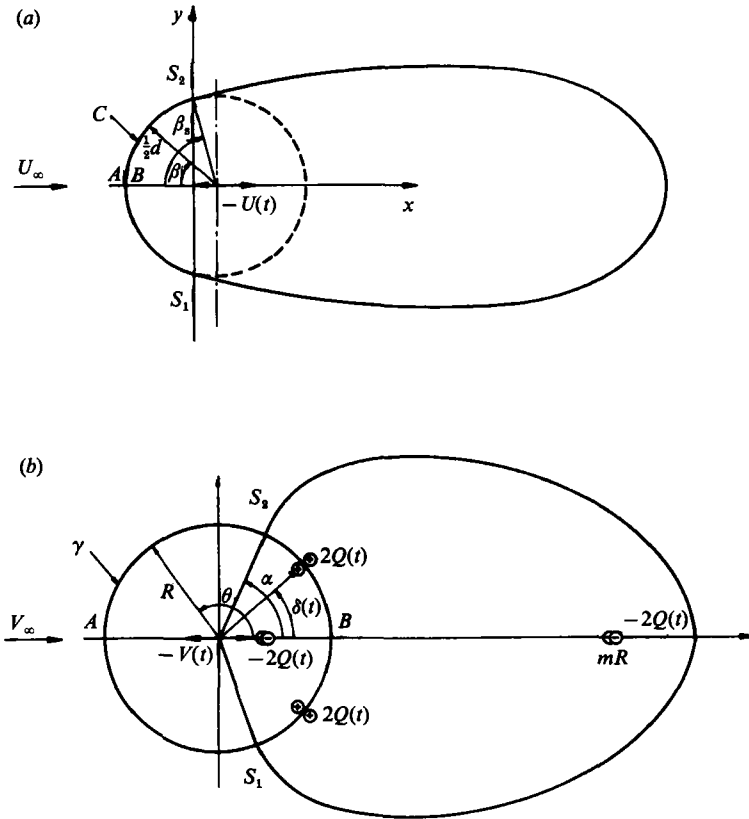
FIGURE 1. (a) Physical z-plane and (b) Parkinson & Jandali's transformed ζ-plane.

m is to be determined. The corresponding image sinks and sources are placed in the circle γ in accordance with Milne-Thomson (1968, §§8.60–8.61).

The complex potential of the resulting flow with respect to the inertial frame of reference (as viewed by a stationary observer outside the circle) is

$$F(\zeta, t) = V_\infty\,\zeta + (V_\infty + V(t))\frac{R^2}{\zeta} + \frac{Q(t)}{\pi}\Big[\ln\,(\zeta - R\,e^{i\delta})$$

$$+ \ln\,(\zeta - R\,e^{-i\delta}) - \ln\Big(\zeta - \frac{R}{m}\Big) - \ln\,(\zeta - mR)\Big]. \quad (2)$$

It should be noted that the cylindrical coordinate ζ (defined as $re^{i\theta}$) is body-centred. Therefore, the sources and sinks in the wake are attached to the ζ-plane of the oscillating circle γ.

The corresponding complex velocity in the ζ-plane is

$$W(\zeta, t) = \frac{\mathrm{d}F}{\mathrm{d}\zeta} = V_\infty + (V_\infty + V(t))\Big(-\frac{R^2}{\zeta^2}\Big)$$

$$+ \frac{Q(t)}{\pi}\Big[\frac{1}{\zeta - R\,e^{i\delta}} + \frac{1}{\zeta - R\,e^{-i\delta}} - \frac{1}{\zeta - R/m} - \frac{1}{\zeta - mR}\Big]. \quad (3)$$

The complex potential has the same value at corresponding points of the Z-plane and

ζ-plane, whereas the complex velocity in the physical Z-plane is related to that in the ζ-plane by

$$W(Z,t) = \frac{W(\zeta, t)}{f'(\zeta)}. \tag{4}$$

Taking $\zeta = Re^{i\theta}$ at the surface of the circle γ, (2) and (3) can be simplified to

$$F(\theta, t) = V_\infty 2R \cos\theta + V(t)R\,e^{-i\theta} + \frac{Q(t)}{\pi} \ln\left|\frac{\cos\theta - \cos\delta}{\cos\theta - c}\right| \tag{5}$$

and

$$W(\theta, t) = V_\infty(1 - e^{-i2\theta}) + V(t)(-e^{-i2\theta}) + \frac{Q(t)}{\pi R}\frac{ie^{-i\theta}\sin\theta}{(\cos\theta - \cos\delta)}\frac{(\cos\delta - c)}{(\cos\theta - c)}, \tag{6}$$

where $c = \frac{1}{2}[m + (1/m)]$.

The unsteady Bernoulli equation is required to obtain the pressure distribution on the surface of the oscillating cylinder shown in figure 1 (*a*). The unsteady Bernoulli equation, written in a body-centred cylindrical coordinate system, is applied to the flow with respect to the oscillating cylinder (a moving frame of reference). Robertson (1965, §5.2) and Milne-Thomson (1968, §3.61) showed this to be written, in our notation as

$$C_p(\theta, t) = \frac{P(\theta, t) - P_\infty}{\frac{1}{2}\rho U_\infty^2} = \frac{U_{r\infty}^2(t) - U_{rel}^2(\theta, t)}{U_\infty^2} - \frac{2}{U_\infty^2}\frac{\partial\phi}{\partial t}\bigg|_s, \tag{7}$$

where $P(\theta, t)$ denotes the unsteady surface pressure distribution and P_∞ the steady free-stream pressure. $U_{r\infty}(t)$ and $U_{rel}(\theta, t)$ denote the magnitude of the incoming stream velocity and surface relative velocity respectively, as viewed by an observer moving with the oscillating cylinder.

Note that $\partial\phi/\partial t|_s$ represents the unsteady velocity potential evaluated at the circular cylinder surface with respect to the inertial frame of reference.

$C_p(\theta, t)$ is expressed in terms of angle θ on the ζ-plane instead of the physical angle β for convenience. By inspection of (7), it can be seen that the surface relative velocity and the unsteady potential terms are required to solve for $C_p(\theta, t)$.

2.1. *Surface relative velocity term* $U_{rel}(\theta, t)$

In general, a fluid particle moving with absolute velocity V_{abs} as seen in a frame of reference moving with velocity $-V(t)$ has a relative velocity given by

$$V_{rel} = V_{abs} + V(t). \tag{8}$$

Therefore, upon substituting the absolute complex velocity of (6) into (8), the complex surface velocity relative to the oscillating cylinder in the ζ-plane can be shown to be

$$W_{rel}(\theta, t) = 2ie^{-i\theta}\sin\theta\left[V_{r\infty}(t) + \frac{Q(t)}{2\pi R}\frac{1}{(\cos\theta - \cos\delta)}\frac{(\cos\delta - c)}{(\cos\theta - c)}\right], \tag{9}$$

where $V_{r\infty}(t) = V_\infty + V(t)$. The surface relative velocity $U_{rel}(\theta, t)$ in the physical Z-plane is then obtained from the corresponding $W_{rel}(\theta, t)$ in the ζ-plane through (4).

The contour of circle γ in the ζ-plane is mapped to the slit $S_1 A S_2 B S_1$ in the physical Z-plane, as written in the body-centred cylindrical-coordinate system, by the analytic function

$$Z = f(\zeta) = K\left[(\zeta - \cot\alpha) - \frac{1}{(\zeta - \cot\alpha)}\right], \tag{10}$$

where K is a scaling factor for different sizes of circular cylinder and α the stagnation angle in the ζ-plane, which corresponds to the separation angle β_s in the Z-plane.

In the above transformation, the relationship between angle β_s in the Z-plane and angle α in the ζ-plane is given by

$$\alpha = \tfrac{1}{2}(\pi - \beta_s). \tag{11}$$

For convenience, the radius R of the circle γ in the ζ-plane is taken to be

$$R = \operatorname{cosec} \alpha. \tag{12}$$

The scaling factor K is related to the separation angle and the diameter of the cylinder by

$$K = \tfrac{1}{4}d \sin \beta_S = \tfrac{1}{2}d \sin \alpha \cos \alpha, \tag{13}$$

where d is the physical diameter of the cylinder in the Z-plane. In the conformal mapping, the separation locations S_1 and S_2 are made critical points at which $f'(\zeta) = 0$. Owing to doubling of angles at the critical points, the normal stagnation streamlines in the ζ-plane will correspond to tangential separation streamlines in the Z-plane. According to (4), $U_{\mathrm{rel}}(\theta, t)$ at these two locations would be infinite, causing the pressure there to be infinite, which is physically inadmissible. Therefore, the first boundary condition will correspond to setting $W_{\mathrm{rel}}(\theta, t) = 0$ at S_1 and S_2 and a relationship between $Q(t)$ and δ is thus obtained:

$$Q(t) = 2\pi V_{\mathrm{r}\infty}(t) \operatorname{cosec} \alpha \, (\cos \delta - \cos \alpha) \frac{(\cos \alpha - c)}{(\cos \delta - c)}. \tag{14}$$

It should be noted that δ is time-dependent. By substituting $Q(t)$ into $W_{\mathrm{rel}}(\theta, t)$, and introducing $\epsilon_0 = (\cos \alpha - c)/(\cos \theta - c)$, we have

$$W_{\mathrm{rel}}(\theta, t) = 2V_{\mathrm{r}\infty}(t) \, \mathrm{i} e^{-\mathrm{i}\theta} \sin \theta \left[1 + \frac{\cos \delta - \cos \alpha}{\cos \theta - \cos \delta} \epsilon_0 \right]. \tag{15}$$

The derivative of the mapping function of (10) on the circle γ is

$$f'(\zeta) = K \left[1 + \frac{\sin^2 \alpha}{(e^{\mathrm{i}\theta} - \cos \alpha)^2} \right]. \tag{16}$$

By substituting (15) and (16) into (4), we arrive at

$$\frac{U_{\mathrm{rel}}(\theta, t)}{V_{\mathrm{r}\infty}(t)} = \frac{|W_{\mathrm{rel}}(\theta, t)|}{|f'(\zeta)| V_{\mathrm{r}\infty}(t)} = \frac{\sin \theta (1 - 2 \cos \theta \cos \alpha + \cos^2 \alpha)\epsilon}{K(\cos \delta - \cos \theta)}, \tag{17}$$

where $\epsilon = [\epsilon_0 \cos \alpha - \cos \theta + (1 - \epsilon_0) \cos \delta]/(\cos \alpha - \cos \theta)$. Since $f'(\zeta) = K$ at infinity, the magnitude of the incoming stream velocities with respect to the oscillating frame of reference, $V_{\mathrm{r}\infty}(t)$ in the ζ-plane and $U_{\mathrm{r}\infty}(t)$ the Z-plane, are related by

$$V_{\mathrm{r}\infty}(t) = KU_{\mathrm{r}\infty}(t) = K \left[U_{\infty} + U(t) \right], \tag{18}$$

and (17) can be further reduced to

$$\frac{U_{\mathrm{rel}}(\theta, t)}{U_{\mathrm{r}\infty}(t)} = \frac{\sin \theta \, (1 - 2 \cos \theta \cos \alpha + \cos^2 \alpha)\epsilon}{(\cos \delta - \cos \theta)}. \tag{19}$$

Equation (19) is the surface relative velocity of an oscillating cylinder in steady mean flow.

2.2. *Unsteady potential term,* $\partial\phi/\partial t\,|_s$

From the definition of the complex potential

$$\phi = \mathrm{Re}\,\{F(\zeta, t)\},$$

we have

$$\frac{\partial\phi}{\partial t} = \mathrm{Re}\left\{\frac{\partial F(\zeta, t)}{\partial t}\right\}. \tag{20}$$

The unsteady potential term on the circle γ can be obtained by differentiating (5) with respect to time and retaining only the real parts to give

$$\frac{\partial\phi}{\partial t}\bigg|_s = \dot{V}(t)\,\mathrm{cosec}\,\alpha\cos\theta + \dot{Q}(t)\frac{1}{\pi}\ln\left|\frac{\cos\theta-\cos\delta}{\cos\theta-c}\right| + \frac{Q(t)}{\pi}\frac{\sin\delta}{(\cos\theta-\cos\delta)^2}\dot{\delta}. \tag{21}$$

The derivative of the source strength can be obtained from (14), noting that $\dot{V}_{r\infty}(t) = \dot{V}(t)$, as

$$\dot{Q}(t) = \dot{V}(t)\,2\pi\,\mathrm{cosec}\,\alpha\,(\cos\delta-\cos\alpha)\frac{(\cos\alpha-c)}{(\cos\delta-c)}$$

$$-V_{r\infty}(t)\,2\pi\,\mathrm{cosec}\,\alpha\sin\delta\,\dot{\delta}\frac{(\cos\alpha-c)^2}{(\cos\delta-c)^2}. \tag{22}$$

By substituting (13), (14), (18) and (22) into (21), the unsteady potential on the circle γ becomes

$$\frac{\partial\phi}{\partial t}\bigg|_s = \dot{U}(t)\,d\cos\alpha\left[\tfrac{1}{2}\cos\theta + (\cos\delta-\cos\alpha)\frac{(\cos\alpha-c)}{(\cos\delta-c)}\ln\left|\frac{\cos\theta-\cos\delta}{\cos\theta-c}\right|\right]$$

$$+ U_{r\infty}(t)\,d\cos\alpha\sin\delta\frac{(\cos\alpha-c)}{(\cos\delta-c)}\dot{\delta}\left[\frac{(\cos\delta-\cos\alpha)}{(\cos\theta-\cos\delta)} - \frac{(\cos\alpha-c)}{(\cos\delta-c)}\ln\left|\frac{\cos\theta-\cos\delta}{\cos\theta-c}\right|\right]. \tag{23}$$

2.3. *Pressure distribution for a circular cylinder oscillating in mean flow*

The unsteady Bernoulli equation as given by (7) is used together with (19) and (23) to obtain the pressure distribution on the front wetted surface of an oscillating circular cylinder as follows:

$$C_p(\theta, t) = \frac{U_{r\infty}^2(t)}{U_\infty^2}\left[1 - \frac{\sin^2\theta(1-2\cos\alpha\cos\theta+\cos^2\alpha)^2\epsilon^2}{(\cos\delta-\cos\theta)^2}\right]$$

$$-\frac{\dot{U}(t)\,d}{U_\infty^2}\left[\cos\alpha\cos\theta + 2\cos\alpha\,(\cos\delta-\cos\alpha)\frac{(\cos\alpha-c)}{(\cos\delta-c)}\ln\left|\frac{\cos\theta-\cos\delta}{\cos\theta-c}\right|\right]$$

$$-\frac{U_{r\infty}(t)}{U_\infty}\frac{d}{U_\infty T}\frac{d\delta}{d(t/T)}2\cos\alpha\sin\delta\frac{(\cos\alpha-c)}{(\cos\delta-c)}\left[\frac{(\cos\delta-\cos\alpha)}{(\cos\theta-\cos\delta)}\right.$$

$$\left.-\frac{(\cos\alpha-c)}{(\cos\delta-c)}\ln\left|\frac{\cos\theta-\cos\delta}{\cos\theta-c}\right|\right]. \tag{24}$$

The angular position β on C corresponding to θ on γ is given from (10) by

$$\sin\beta = \cos\alpha\sin\theta\left[\frac{\sec\alpha-\cos\theta}{\tfrac{1}{2}(\sec\alpha+\cos\alpha)-\cos\theta}\right]. \tag{25}$$

For the case where the cylinder is performing simple harmonic motion with

amplitude r and angular velocity ω in steady mean flow, the velocity and acceleration are given by

$$U_{r\infty}(t) = U_\infty + r\omega \sin \omega t, \tag{26}$$

$$\dot{U}(t) = r\omega^2 \cos \omega t. \tag{27}$$

Hence, the pressure coefficient is given by

$$C_p(\theta, t) = \left(1 + \frac{r\omega}{U_\infty} \sin \omega t\right)^2 \left[1 - \frac{\sin^2 \theta (1 - 2\cos\alpha \cos\theta + \cos^2\alpha)^2 \epsilon^2}{(\cos\delta - \cos\theta)^2}\right.$$

$$- \frac{r\omega^2 d}{U_\infty^2} \cos \omega t \left[\cos\alpha \cos\theta + 2\cos\alpha (\cos\delta - \cos\alpha) \frac{(\cos\alpha - c)}{(\cos\delta - c)} \ln \left|\frac{\cos\theta - \cos\delta}{\cos\theta - c}\right|\right]$$

$$- \left(1 + \frac{r\omega}{U_\infty} \sin \omega t\right) \frac{d}{U_\infty T} \frac{d\delta}{d(t/T)} 2\cos\alpha \sin\delta \frac{(\cos\alpha - c)}{(\cos\delta - c)}$$

$$\times \left[\frac{(\cos\delta - \cos\alpha)}{(\cos\theta - \cos\delta)} - \frac{(\cos\alpha - c)}{(\cos\delta - c)} \ln \left|\frac{\cos\theta - \cos\delta}{\cos\theta - c}\right|\right]. \tag{28}$$

It can be seen that the above expression is a first-order nonlinear differential equation. It involves the source angle $\delta(t)$ and the stagnation angle α besides the basic parameters r, ω and U_∞. The angles θ, α, δ are not transformed back to the physical Z-plane to preserve the simplicity of the above expression.

For steady flow past a circular cylinder,

$$\frac{U_{r\infty}(t)}{U_\infty} = 1.0, \quad \dot{U}(t) = 0.$$

Furthermore, the strength and angular positions of the sources do not change, and thus the derivative of the source angle is zero. With these conditions, (28) reduces to

$$C_p(\theta) = \left[1 - \frac{\sin^2 \theta (1 - 2\cos\alpha \cos\theta + \cos^2\alpha)^2 \epsilon^2}{(\cos\delta - \cos\theta)^2}\right]. \tag{29}$$

3. Method of solution

There are altogether three unknowns in the unsteady wake-source model: the constant parameter m which is related to the location of the sinks behind the body, the source strength $Q(t)$ and the angular position δ which is time-dependent.

The sinks were placed downstream behind the body for flow continuity in order to satisfy the zero unsteady potential requirement at infinity for irrotational flow modelling, as explained in Sarpkaya & Issacson (1981, p. 28). This is because in the far field the irrotational-flow pressure disturbance caused by the body's presence must be zero.

The location parameter m of the downstream sinks is determined from the criterion of continuous separation pressure in steady-flow solution of the closed-wake model. Detailed experimental studies and documentations of steady flow past circular cylinders and flat plates were carried out by Cantwell & Coles (1983) and Fage & Johansen (1927) respectively. It was observed that the phase-averaged pressure along the separation streamlines increase monotonically from the separation pressure value, at the separation locations, towards the free-stream pressure value downstream of the bluff bodies. This criterion is thus used to determine the location of the downstream sinks. With an initial estimated location of sinks near the body, the pressure distribution around the circular cylinder and along the separation

streamlines are computed. The pressure distribution functions along the separation streamline were found to contain a discontinuity (a sharp drop in pressure) immediately downstream of the separation location, which is physically inadmissible, if the sinks were placed too close to the body. The location of the sinks is then varied and the computation of pressure distribution is repeated until a smooth and gradually increasing pressure distribution function along the separation streamlines is obtained. This location corresponds to a critical value of m beyond which the pressure distribution function does not contain any discontinuity. It has been verified that varying the value of m beyond this has negligible effect on the pressure distribution on the front wetted surface of the circular cylinder.

For a given set of empirical C_{pb} and β_s, it is interesting to note that the critical value of m remains unchanged with different free-stream flow velocity and circular cylinder radius. This is because the strength of the sinks downstream is directly proportional to the relative velocity of the incoming flow and the radius of the cylinder as given by (14). Since a closed-wake model is necessary, as explained earlier, the sinks are fixed at this critical location when the model is extended to unsteady flow.

In the close-wake modelling, there exists a stagnation point somewhere downstream of the sinks whereas there is a far-wake displacement thickness in the real flow. The location of the stagnation point is dependent on the strength and the location mR of the sinks discussed above. We shall allow the existence of the said stagnation point since it does not affect the solution in the near vicinity of the circular cylinder, which is of interest in the present paper.

Two more boundary conditions are required for a unique solution. The first one corresponds to setting $W_{rel}(\theta, t) = 0$ at S_1 and S_2, as in §2.1, to obtain (14) which allows the unknowns $Q(t)$ and $\dot{Q}(t)$ in the unsteady potential term to be replaced such that the $C_p(\theta, t)$ can be expressed in δ and $\dot{\delta}$ only. The second boundary condition is to satisfy the separation pressure condition. As stated in assumption (v), the time-dependent phase-averaged separation pressure is assumed to be the time-dependent uniform phase-averaged back pressure over the body surface. By setting $\theta = \alpha$ in (24), the back pressure equation is obtained as

$$
\begin{aligned}
C_{pb}(t) = {} & \frac{U_{r\infty}^2(t)}{U_\infty^2}\left[1 - \frac{\sin^6\alpha}{(\cos\delta - \cos\alpha)^2}\right] \\
& - \frac{\dot{U}(t)\,d}{U_\infty^2}\left[\cos^2\alpha + 2\cos\alpha\,(\cos\delta - \cos\alpha)\frac{(\cos\alpha - c)}{(\cos\delta - c)}\ln\left|\frac{\cos\alpha - \cos\delta}{\cos\alpha - c}\right|\right] \\
& + \frac{U_{r\infty}(t)}{U_\infty}\frac{d}{U_\infty T}\frac{\mathrm{d}\delta}{\mathrm{d}(t/T)}2\cos\alpha\sin\delta\frac{(\cos\alpha - c)}{(\cos\delta - c)} \\
& \times \left[1 + \frac{(\cos\alpha - c)}{(\cos\delta - c)}\ln\left|\frac{(\cos\alpha - \cos\delta)}{(\cos\delta - c)}\right|\right].
\end{aligned}
\tag{30}
$$

The above first-order nonlinear differential equation in δ can be solved numerically by using the fourth-order Runge–Kutta algorithm with arbitrarily specified initial condition at $t = 0$. The cylinder is assumed to start from rest and gradually approaches $r\omega\sin\omega t$ in an exponential manner. The initial source angle is assumed to be $15°$, as obtained from the steady-flow solution. However, this initial value is not important, as the source angle δ will converge to the correct value when steady oscillation is reached. The time interval is chosen to be $T/2000$. A Fortran program was developed and run on the IBM3081 mainframe to solve the differential equation.

4. Derivation of drag and added-mass coefficients

In the following part of this paper, through the unsteady wake-source model, the derivation of the instantaneous drag coefficient $C_D(t)$, and instantaneous added-mass coefficient $C_A(t)$ (hence the instantaneous inertia coefficient $C_M(t)$) are shown. For symmetrical flow, the in-line force coefficient $C_F(t)$ can be obtained by integrating the pressure distribution over the circular cylinder as

$$C_F(t) = \frac{F(t)}{\frac{1}{2}\rho U_\infty^2 d} = \int_0^\pi C_p(\beta, t)\cos\beta\,d\beta, \tag{31}$$

where β is the physical angle measured from the front stagnation point. Since the back pressure is assumed uniform, i.e. independent of β, (31) can be further simplified to

$$C_F(t) = \int_0^{\beta_s} C_p(\beta, t)\cos\beta\,d\beta - C_{pb}(t)\sin\beta_s. \tag{32}$$

Since the pressure distribution as given in (28) is expressed in terms of the parametric variable θ, by using (25) and (28) we obtain

$$C_F(t) = \int_\pi^\alpha C_p(\theta, t)\,g(\theta)\,d\theta - C_{pb}(t)\sin\beta_s, \tag{33}$$

where
$$g(\theta) = \frac{\sin^2\theta\,(\cos\alpha\cos\theta - 1)}{[\frac{1}{2}(\sec\alpha + \cos\alpha) - \cos\theta]^2} + \frac{\cos\theta - \cos\alpha\cos 2\theta}{\frac{1}{2}(\sec\alpha + \cos\alpha) - \cos\theta}.$$

Some physical interpretations of $C_{pb}(t)$ are considered before solving for $C_F(t)$. First, (28) is re-written as follows:

$$C_p(\theta, t) = f_1(\theta, t)\left(1 + \frac{r\omega}{U_\infty}\sin\omega t\right)^2 + f_2(\theta, t)\frac{\pi}{2}\frac{r\omega^2 d}{U_\infty^2}\cos\omega t + f_3(\theta, t)\left(1 + \frac{r\omega}{U_\infty}\sin\omega t\right), \tag{34}$$

where
$$f_1(\theta, t) = \left[1 - \frac{\sin^2\theta\,(1 - 2\cos\alpha\cos\theta + \cos^2\alpha)^2\epsilon^2}{(\cos\delta - \cos\theta)^2}\right],$$

$$f_2(\theta, t) = -\frac{2}{\pi}\left[\cos\alpha\cos\theta + 2\cos\alpha\,(\cos\delta - \cos\alpha)\frac{(\cos\alpha - c)}{(\cos\delta - c)}\ln\left|\frac{\cos\theta - \cos\delta}{\cos\theta - c}\right|\right]$$

and
$$f_3(\theta, t) = -\frac{d}{U_\infty T}\frac{d\delta}{d(t/T)}2\cos\alpha\sin\delta\frac{(\cos\alpha - c)}{(\cos\delta - c)}\left[\frac{(\cos\delta - \cos\alpha)}{(\cos\theta - \cos\delta)}\right.$$
$$\left. - \frac{(\cos\alpha - c)}{(\cos\delta - c)}\ln\left|\frac{\cos\theta - \cos\delta}{\cos\theta - c}\right|\right].$$

It can be seen from (34) that the pressure acting at a point on the front wetted surface is made up of two components:

(i) The term corresponding to $f_1(\theta, t)$ which is derived from consideration of tangential velocity relative to the surface of the oscillating cylinder.

(ii) The inertia terms: $f_2(\theta, t)$ and $f_3(\theta, t)$, both obtained from the time derivative of the surface velocity potential, $\partial\phi/\partial t|_s$, which corresponds to the local temporal acceleration of the surface flow. These are assumed to be zero because the inertia effect in the wake is neglected.

With this assumption, the empirically obtained back pressure coefficient $C_{pb}(t)$ can

be used together with (34) to solve for (33). The in-line force coefficient equation can then be expressed as

$$C_F(t) = \left[\int_\pi^\alpha f_1(\theta, t)\, g(\theta)\, \mathrm{d}\theta - h_1(t)\sin\beta_s \right]\!\left(1 + \frac{r\omega}{U_\infty}\sin\omega t\right)^2$$

$$+ \left[\int_\pi^\alpha f_2(\theta, t)\, g(\theta)\, \mathrm{d}\theta \right]\frac{\pi}{2}\frac{r\omega^2 d}{U_\infty^2}\cos\omega t$$

$$+ \left[\int_\pi^\alpha f_3(\theta, t)\, g(\theta)\, \mathrm{d}\theta \right]\!\left(1 + \frac{r\omega}{U_\infty}\sin\omega t\right), \qquad (35)$$

where
$$h_1(t) = \frac{C_{pb}(t)}{(1 + (r\omega/U_\infty)\sin\omega t)^2}.$$

However, when the familiar Morison's equation is applied to the present flow, the in-line force coefficient $C_F(t)$ for an oscillating cylinder in a steady mean flow can be written as

$$C_F(t) = \frac{F(t)}{\frac{1}{2}\rho U_\infty^2 d} = C_D\!\left(1 + \frac{r\omega}{U_\infty}\sin\omega t\right)^2 + C_A\frac{\pi}{2}\frac{r\omega^2 d}{U_\infty^2}\cos\omega t, \qquad (36)$$

where $F(t)$ is the in-line force. The average hydrodynamic drag and added-mass coefficients, C_D and C_A, are conventionally determined empirically using least-squares or Fourier analysis methods which yield similar results (Sarpkaya & Issacson 1981). These coefficients are usually expressed in terms of Keulegan–Carpenter number KC (defined as $2\pi r/d$), the reduced velocity U_r (defined as $U_\infty T/d$, where T is the period of oscillation), the Reynolds number based on the maximum velocity Re_m and the frequency parameter β_f (defined as $d^2/\nu T$, where ν is the kinematic viscosity of the fluid).

It should be noted that the relationship between the added-mass coefficient $C_A(t)$, and the inertia coefficient $C_M(t)$ for the case of superimposed oscillatory and mean low past a stationary cylinder, is given by

$$C_M(t) = 1 + C_A(t). \qquad (37)$$

Equation (37) is equally applicable when the average values of C_M and C_A are used instead of the instantaneous values.

Interestingly, when (35) is compared with the Morison's equation as in (36), it can be seen that they are compatible with the variables in the square-brackets expressed in terms of coefficients as

$$C_F(t) = C_D(t)\!\left(1 + \frac{r\omega}{U_\infty}\sin\omega t\right)^2 + C_A(t)\frac{\pi}{2}\frac{r\omega^2 d}{U_\infty^2}\cos\omega t + C_R(t)\!\left(1 + \frac{r\omega}{U_\infty}\sin\omega t\right). \qquad (38)$$

Thus, the instantaneous drag and added-mass coefficients, derived from the unsteady wake-source model, are defined as

$$C_D(t) = \int_\pi^\alpha f_1(\theta, t)\, g(\theta)\, \mathrm{d}\theta - h_1(t)\sin\beta_s, \qquad (39)$$

$$C_A(t) = \int_\pi^\alpha f_2(\theta, t)\, g(\theta)\, \mathrm{d}\theta. \qquad (40)$$

The corresponding instantaneous inertia coefficient is obtained using (37)

$$C_M(t) = 1 + \int_\pi^\alpha f_2(\theta, t)\, g(\theta)\, \mathrm{d}\theta. \qquad (41)$$

It is noted that an additional term is present in $C_F(t)$, (38), when the unsteady wake-source model is used. The corresponding coefficient of this term is derived from $\partial\phi/\partial t|_s$ which is related to the inertia of the flow. This coefficient, as well as the corresponding term, is found to be very small. Therefore, it is tentatively called the residual-inertial coefficient and defined as

$$C_R(t) = \int_\pi^\alpha f_3(\theta, t)\, g(\theta)\, \mathrm{d}\theta. \tag{42}$$

The above-defined coefficients are dependent on the source angle $\delta(t)$ and can be readily obtained by numerical integration after $\delta(t)$ is solved in §3.

5. The experiment

In order to provide empirical inputs to the present unsteady wake-source model and experimental data for comparison, an experiment was conducted to measure the phase-averaged pressure distributions around a circular cylinder oscillating along the direction of free-stream flow in a wind tunnel. Most of the published experiments on unsteady flow around a cylinder involved the measurements of force rather than pressure. However, Matten (1979) measured, with 24 pressure transducers, the instantaneous pressure distribution around a circular cylinder oscillating in simple harmonic motion while being towed along the direction of oscillation in a tow tank. In the present experiment, the phase-averaged pressure distribution over several oscillations are measured around the cylinder, instead of the instantaneous value.

The experiment was conducted in an open-circuit wind tunnel of cross-section 1 m high, 2 m wide and free-stream turbulence intensity below 0.15%. A circular cylinder of 0.1 m diameter and 0.95 m length, with end plates of 0.3 m diameter, was oscillated along the direction of free-stream flow by a Scotch-yoke mechanism on top of the wind tunnel. The frequency of oscillation and free-stream velocity were varied up to 110 r.p.m. and 8.5 m/s respectively.

The pressure at the mid-span of the cylinder was measured by a Setra model 237 strain-gauge pressure transducer of 689 N/m² (0.1 p.s.i.) range via a 1 mm diameter pressure tapping. The transducer was mounted inside the cylinder and connected to the pressure tapping via a 50 mm length of plastic tubing. In order to reduce the response time of the pressure transducer, the plastic tubing was kept short and the air trapped between the adapter housing and the pressure transducer diaphragm was kept to a minimum. Based on the method of Archibald & Robins (1952), the time lag in the pressure measuring system was found to be about 2.2 ms which is insignificant when compared to the rate of data acquisition and the cylinder's speed of oscillation. The pressure signal was amplified, converted to a digital signal and acquired by an Apple II microcomputer.

To synchronize the pressure transducer signal with the oscillation of the cylinder, two pulse trains were generated using a perforated disc, a photo-transistor and a light source. The sampling pulse train was generated by 100 equally-spaced peripheral holds on the perforated plate attached to the shaft carrying the Scotch-yoke mechanism. A light source and a photo-transistor were aligned with the hole on each side of the disc and the intermittent interruption of the light generated a sampling pulse train at 100 times the frequency of oscillation. The sampling pulse train was converted to a TTL signal using Schmidt's trigger and fed to the microcomputer to trigger the sampling of pressure signal at 100 equal time intervals t in a time period T of oscillation.

In order to begin sampling at a reference oscillation position, a second triggering pulse train was generated by having a reference hole on the same perforated disc aligned radially with one of the 100 sampling holes. This reference hole, together with a light source and a photo-transistor, generated a triggering pulse train at the same frequency as the cylinder's oscillation. The triggering pulse was converted to a TTL signal by a Schmidt's trigger and fed to a R–S flip-flop circuit so that after manual initialization, the sampling could begin when the first trigger pulse was detected. In the present investigation, the sampling of the pressure signal began when the cylinder was at the extreme downstream position of an oscillation. The pressure signal was phase-averaged over 20 oscillations. It was found that 20 oscillations were sufficient for the phase-averaged pressure to attain a stationary mean.

The pressure distribution around the cylinder was obtained by positioning the pressure tapping at $10°$ intervals from $0°$ to $180°$. The 19 sets of phase-averaged pressure data, although taken at different times but referenced to the same phase of oscillation, could be used to construct the mean pressure distribution around the cylinder at $\frac{1}{100} T$ time interval. The normalized mean pressure distribution curves in the form of the pressure coefficient $C_p(t)$ at different oscillation phases t/T were used to provide empirical inputs to the present unsteady wake-source model and experimental data for comparison. The detailed experimental set-up and some of the experimental results are presented in Low, Chew & Tan (1989).

6. Results and discussion

6.1. *Verification of closed-wake model*

The present closed-wake model is verified by comparison of the computed pressure distributions with the measurements of the present experiment and those obtained by previous investigators for the case of a stationary cylinder in steady flow. The computed pressure distributions as shown in figure 2 are based on a separation angle of $80°$ and averaged back pressure coefficient of -1.05. These computed results agree well with the present experimental measurements taken at Reynolds numbers 27 000 and 54 000 respectively. The measurements exhibit the subcritical pressure distributions with the separation angle approximately at $80°$. The computed results also compare well with the experimental measurements of Cantwell & Coles (1983) at Reynolds number 140 000 which has a separation angle at approximately $77°$ and averaged back pressure coefficient of -1.06.

The experiment of Cantwell & Coles (1983) was performed at Reynolds number 140 000 which is higher than the Reynolds numbers of the present experiment. Nevertheless, they are in the subcritical flow regime and the present experimental measurements agree well with theirs. The steady flow drag coefficients, C_{DS}, for the present two cases are 1.26 and 1.13 respectively. They are obtained by integrating the experimental pressure distributions around the circular cylinder without the wind-tunnel blockage or cylinder's aspect ratio correction. These values also compare favourably with the C_{DS} of 1.237 obtained by Cantwell & Coles (1983). This comparison served as a check on the validity of the present experimental set-up before the experiments on an oscillating cylinder were conducted.

As explained in §3, the pressure distributions along the separation streamlines were computed for the determination of parameter m which corresponds to the location of the sinks to close the wake. The present closed-wake model approaches Parkinson & Jandali's original open-wake model if the sinks were placed increasingly
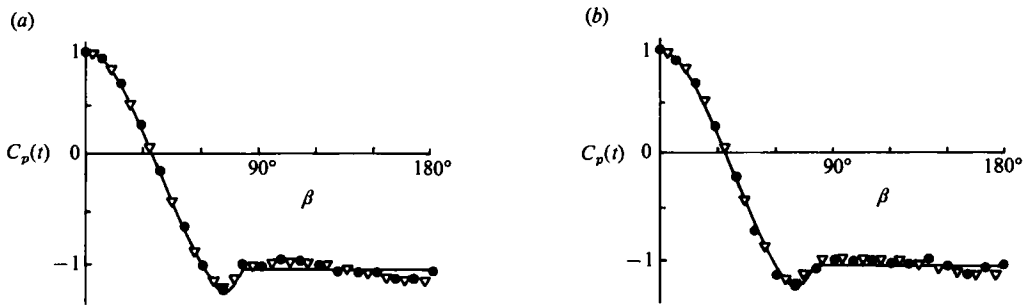
(a)

(b)

FIGURE 2. Comparison of measured and computed steady flow pressure distributions. ●, present experiment, $\beta_s = 80°$, $C_{pb} = -1.05$, (a) $Re = 27000$, (b) $Re = 54000$; ∇, Cantwell & Coles (1983), $Re = 140000$, $\beta_s = 77°$, $C_{pb} = -1.06$; ——, present closed-wake model for steady flow, $m = 17$. (Identical to Parkinson & Jandali's (1970) model.)
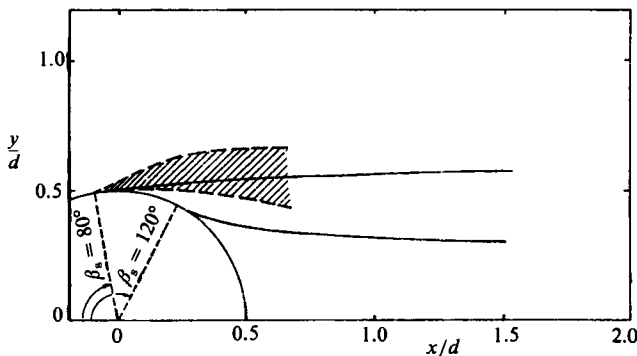

FIGURE 3. Separation streamline shapes for circular cylinder by present model. $\beta_s = 80°$, $C_{pb} = -1.05$, $m = 17$; $\beta_s = 120°$, $C_{pb} = -0.38$, $m = 8.0$. Shaded area, Cantwell & Coles (1983) shear-layer measurements.

further downstream. However, the pressure distribution on the circular surface is found to be indistinguishable from those obtained by Parkinson & Jandali's model.

The separation streamline shapes were also computed for comparison with experimental data as shown in figure 3. For the subcritical flow regime, a separation angle of 80° and back pressure coefficient of -1.05 has an m value of 17. It is interesting to note that the shape of the separation streamline calculated by the present closed-wake model shows good agreement with experimental data obtained by Cantwell & Coles (1983). The separation streamline shape for the supercritical regime is also computed using the data from Parkinson & Jandali (1970). For $\beta_s = 120°$ and $C_{pb} = -0.38$, the corresponding value of m is 8. In the near wake region as shown, these streamlines are indistinguishable from those obtained by Parkinson & Jandali (1970). It should be noted that the streamlines represent the time-averaged separation shear-layers rather than the physical streamlines marking the wake region. Furthermore, the streamlines do not intersect the cylinder surface downstream of separation locations which satisfy the requirements discussed in Parkinson & Jandali (1970, §4.2) and Wood (1955, §4).

6.2. Pressure distribution for a circular cylinder oscillating in mean flow

In the present unsteady wake-source model, the separation angle is assumed to be unaffected by the oscillations of the cylinder. This is supported by the experimental pressure distributions at different phases of oscillation as presented in figures 4–6.
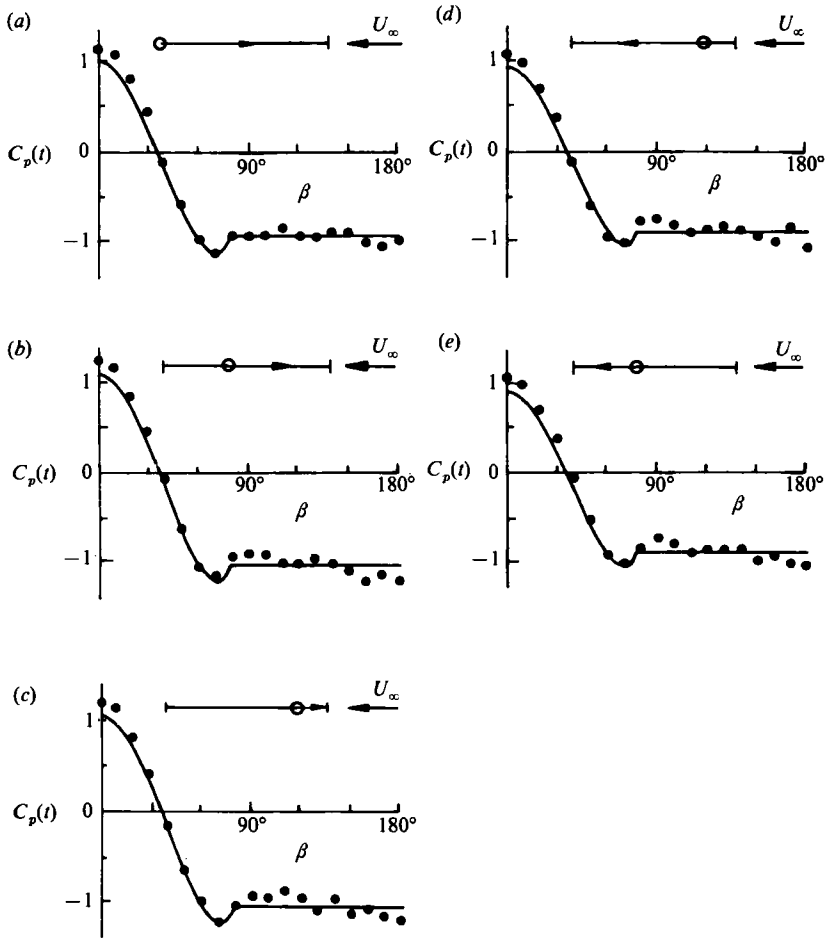
FIGURE 4. Pressure distributions at different phases on circular cylinder oscillating in steady mean flow. ——, present model; ●, present experimental data; $Re = 54000$, $KC = 2.51$, $\beta_f = 1010$, $U_r = 53.7$, $VR = 0.05$; $U_\infty = 8.5$ m/s, $r = 0.04$ m, $\omega = 95$ r.p.m. (a) $t/T = 0$; (b) 0.2; (c) 0.4; (d) 0.6; (e) 0.8.

For the range of parameters investigated, the separation angle appears to be constant at all phases. It is approximately equal to 80°, the value usually observed for steady subcritical Reynolds-number flow past a circular cylinder. Furthermore, all the subsequent unsteady wake-source model results compare favourably with the experimental data when computed with empirical separation angle of 80°.

The experimental measurements of unsteady flow past the cylinder were obtained by varying the amplitude of oscillation r, the frequency of oscillation ω and the mean free-stream velocity U_∞. The amplitude of oscillation can be described by the Keulegan–Carpenter number KC and the frequency of oscillation is characterized by the frequency parameter β_f. The mean free-stream velocity influence is reflected in the Reynolds number Re, defined as $U_\infty d/\nu$.

The combined effects of amplitude, frequency, and mean velocity can be represented by a velocity ratio parameter VR defined as $r\omega/U_\infty$. It represents basically the ratio of maximum oscillation velocity $r\omega$ to the free-stream velocity U_∞
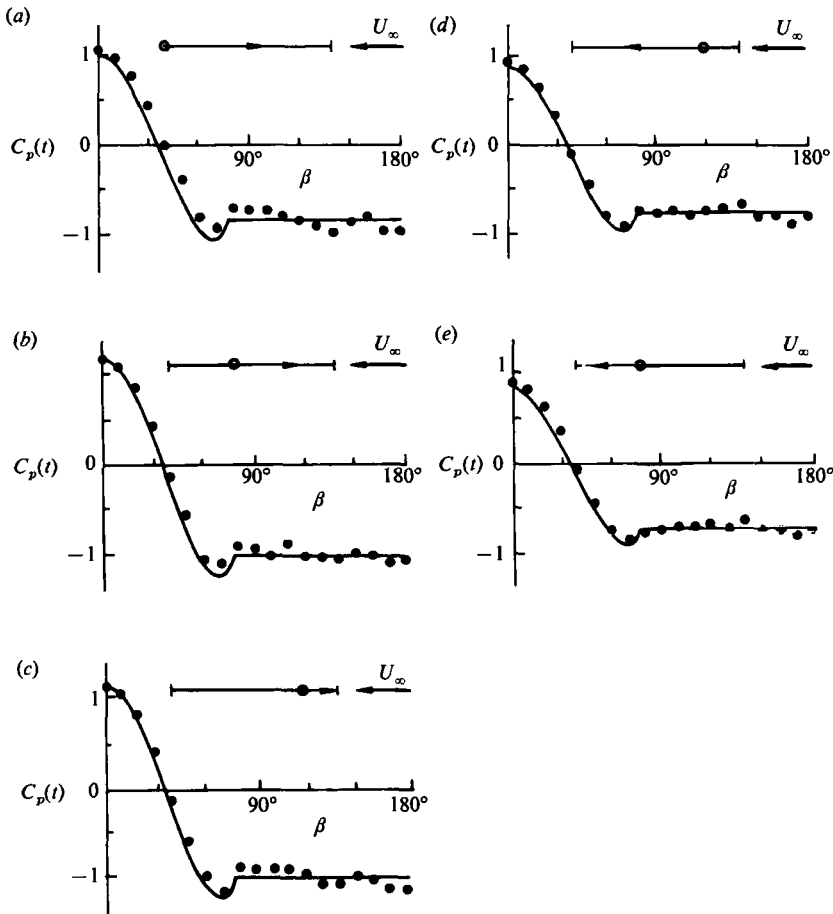
FIGURE 5. Pressure distributions at different phases on circular cylinder oscillating in steady mean flow. ———, present model; ●, present experimental data; $Re = 54000$, $KC = 9.42$, $\beta_f = 521$, $U_r = 104$, $VR = 0.09$; $U_\infty = 8.5$ m/s, $r = 0.15$ m, $\omega = 49$ r.p.m. (a) $t/T = 0$; (b) 0.2; (c) 0.4; (d) 0.6; (e) 0.8.

and indicates the degree of unsteadiness of flow past the cylinder. It is related to KC, β_f and Re by

$$VR = \frac{KC \times \beta_f}{Re}.$$

A relatively small VR is required for the present model to ensure that the shed vortices do not interact directly with the body in order to satisfy the assumptions made. The present model is not expected to be valid for values of VR near to or larger than 1.0.

Another useful parameter to describe the unsteady flow is the reduced velocity U_r. If the time period of oscillation T coincides with the time period of vortex shedding, this number becomes the inverse of the Strouhal number. For flow past a circular cylinder in subcritical Reynolds-number flow, the Strouhal number is approximately 0.2, corresponding to $U_r = 5$. Thus, if the reduced velocity is much greater than 5, it indicates that the frequency of oscillation is much lower than the vortex-shedding frequency and strong coupling of the two effects is not expected. The present unsteady wake-source model is not valid when U_r is close to 5 where there is strong
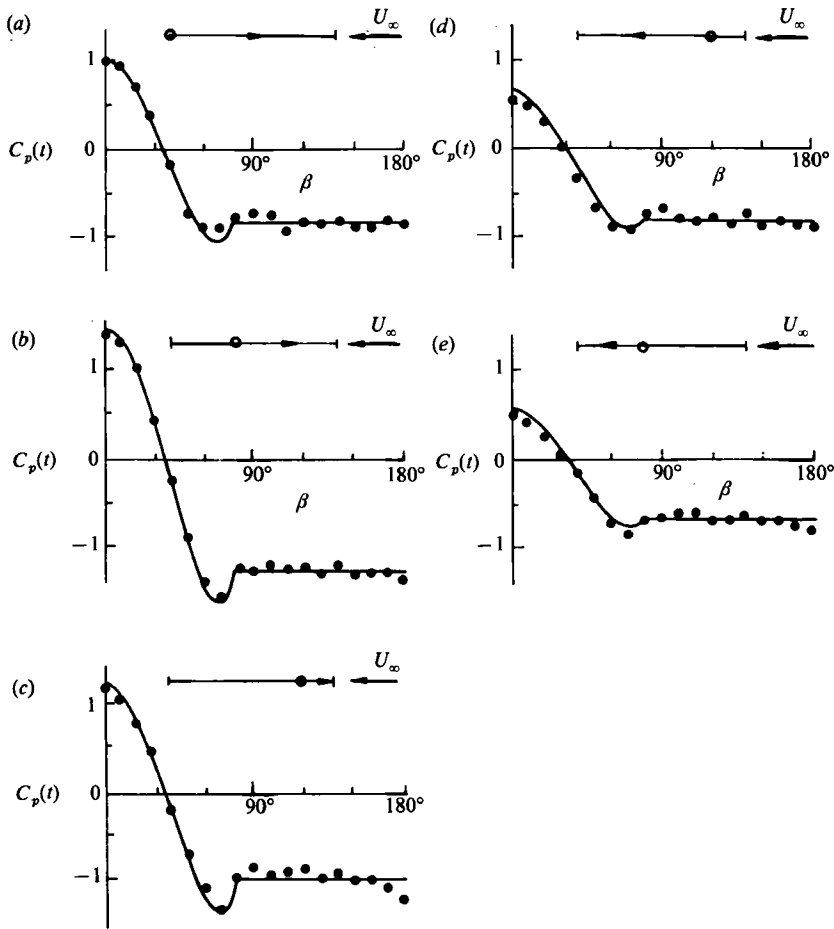
FIGURE 6. Pressure distributions at different phases on circular cylinder oscillating in steady mean flow. ——. present model; ●, present experimental data; $Re = 27000$, $KC = 16.96$, $\beta_t = 393$, $U_r = 68.9$, $VR = 0.25$; $U_\infty = 4.25$ m/s, $r = 0.27$ m, $\omega = 37$ r.p.m. (a) $t/T = 0$; (b) 0.2; (c) 0.4; (d) 0.6; (e) 0.8.

interaction between the oscillation and vortex-shedding frequencies. The reduced velocity is related to KC and VR by

$$U_r = \frac{KC}{VR}.$$

Although there are many sets of measurements taken, only three representative sets which cover the range of experimental variables, r, ω, U_∞ are presented in figures 4–6 to verify the present unsteady wake-source model. Figure 4 represents the measurements at low amplitude and high frequency of oscillation while figure 5 represents the measurements at high amplitude and low frequency of oscillation. In both cases, the computed results from the unsteady wake-source model predict the measured data well at different phases of oscillation except near the front portion of the cylinder in figure 4.

Figure 6 represents measurements at large unsteadiness with $VR = 0.25$. This is reflected in the large variation of the pressure distribution around the cylinder with

the phases of oscillation. The measured stagnation point C_p varies from 1.5 at $t/T = 0.2$ to about 0.5 at $t/T = 0.8$ and the wake C_p varies from -1.25 at $t/T = 0.2$ to about -0.65 at $t/T = 0.8$. However, the computed results still manage to predict the pressure variation reasonably well except for the retreating half of the oscillation when the cylinder is moving away from the flow.

In all three cases presented above, the reduced velocity is much greater than 5 and strong coupling of the vortex-shedding frequency and the cylinder-oscillation frequency is not expected. The experiment cannot be extended to lower reduced velocity because of the difficulty in oscillating a large diameter cylinder at high frequency without introducing the problems of vibration and large variation in motor torque required. It is also difficult to conduct the experiment at low free-stream velocity U_∞ in order to reduce U_r or increase VR since a very sensitive pressure transducer is then required. If experimental measurements are available at lower U_r and higher VR, the present unsteady wake-source model can be further tested in a more demanding flow with large unsteadiness.

6.3. *Variations of in-line force, drag and inertia coefficients over a cycle*

The in-line force coefficient from the unsteady wake-source model is evaluated through (35) and the experimental in-line force coefficient is obtained from the experimental phase-averaged pressure distribution through integration over the circular cylinder surface. Comparison between the theoretical and experimental in-line force coefficients are made in figures 7 and 8. Figure 7 represents the case of low amplitude and high-frequency oscillation (as in figure 4) and figure 8 represents the high unsteady case of high amplitude and high frequency of oscillation (as in figure 6). The present theory predicts the force variation over the cycle satisfactorily.

There have been some attempts to evaluate the variations of instantaneous drag and inertia coefficients from Morison's equation for the case of pure oscillatory flow past circular cylinder. However, these methods of evaluation were not without criticism and therefore not extended to the solving of $C_M(t)$ and $C_D(t)$ for superimposed mean and oscillatory flow past circular cylinder. Keulegan & Carpenter (1958, §8) attempted to evaluate $C_M(t)$ and $C_D(t)$ from Morison's equation together with two other imposed assumptions. Their method is not acceptable (Sarpkaya & Issacson 1981) because there is no distinction between accelerating flow and decelerating flow as long as the absolute values of velocities and accelerations are equal. Sarpkaya & Issacson (1981, §3.87) proposed to determine the variation of $C_M(t)$ and $C_D(t)$ in one oscillating cycle from a set of Morison's equations written at $t = t_n$ and $t = t_n + \Delta t$ assuming that $C_M(t)$ and $C_D(t)$ remain constant in the small time interval Δt. Their method of evaluation is also questionable because when one attempts to evaluate $C_M(t)$ and $C_D(t)$ (two unknowns) from Morison's equation (one equation) without an additional constraint equation (which is not available), there are an infinite number of possible solutions.

The present method of evaluation, from the unsteady wake-source model, will give unique solutions for instantaneous drag coefficient $C_D(t)$ and the corresponding inertia coefficient $C_M(t)$ (see (37) and (41)), as well as the additional residual-inertia coefficient $C_R(t)$. Figures 9 and 10 show the variations of $C_D(t)$, $C_M(t)$ and $C_R(t)$ during a cycle for the two cases considered. It can be seen that there is no particular regularity in the variations of these coefficients over the cycle. The mean drag, inertia and residual-inertia coefficients can be obtained by averaging the respective instantaneous coefficient over the cycle.

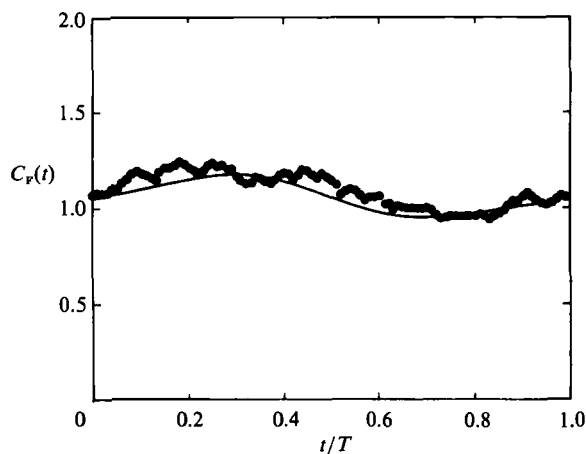The instantaneous value of $C_D(t)$ does not deviate much from the mean drag

FIGURE 7. Comparison of measured and computed in-line force coefficient during an oscillating cycle. ——, present model; ●, present experimental data; $Re = 54\,000$, $KC = 2.51$, $\beta_r = 1010$, $U_r = 53.7$, $VR = 0.05$; $U_\infty = 8.5$ m/s, $r = 0.04$ m, $\omega = 95$ r.p.m.
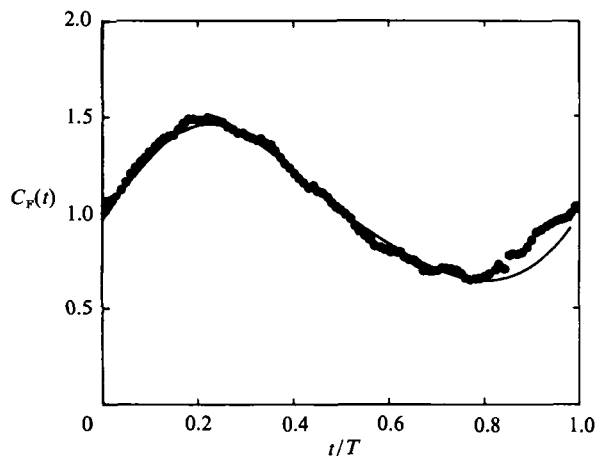

FIGURE 8. Comparison of measured and computed in-line force coefficient during an oscillating cycle. ——, present model; ●, present experimental data; $Re = 27\,000$, $KC = 16.96$, $\beta_r = 393$, $U_r = 68.9$, $VR = 0.25$; $U_\infty = 4.25$ m/s, $r = 0.27$ m, $\omega = 37$ r.p.m.

coefficient C_D of 1.06 for the low VR case, as shown in figure 9. The mean drag coefficient C_D is 1.01 for the high VR case, as shown in figure 10, and the deviation of the instantaneous value from its mean value is also larger. The present results of C_D are consistent with those obtained in previous investigations as shown in table 1.

The instantaneous inertia coefficient for oscillatory flow $C_M(t)$ computed from the present model (see (41)) has negligible variation over the cycle of oscillation, as seen from the two examples in figures 9 and 10. In all the other cases computed, $C_M(t)$ remains approximately constant at its mean C_M of 1.76 throughout. This is because the present unsteady wake-source model is a phase-averaged model which does not account for any possible influence from vortex shedding and fluctuation in the separation location. The present C_M also compares favourably with results obtained in previous investigations, as shown in table 2.

The instantaneous residual-inertia coefficient $C_R(t)$, which is not present in
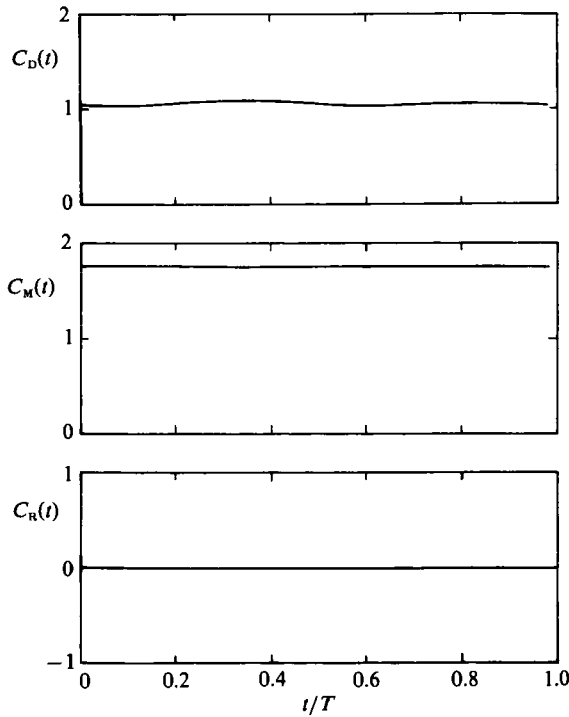
FIGURE 9. An example of computed instantaneous drag, inertia and residual-inertia coefficients during an oscillating cycle. $Re = 54000, KC = 2.51, \beta_t = 1010, U_r = 53.7, VR = 0.05; U_\infty = 8.5$ m/s, $r = 0.04$ m, $\omega = 95$ r.p.m.

Morison's equation, remains insignificant in all the cases investigated. The maximum $C_R(t)$ values during a cycle, as shown in figures 9 and 10, are only of the order of 10^{-3} and their mean values remain approximately zero (of the order of 10^{-6}). From (42), it can be seen that the $C_R(t)$ is proportional to $1/U_r$ and $d\delta/d(t/T)$ which is related to the rate of back pressure variation. In all cases, the reduced velocity is high and the rate of back pressure variation is not large.

For the two examples shown in figures 9 and 10, the instantaneous hydrodynamic coefficients $C_D(t)$, $C_M(t)$ and $C_R(t)$ are shown to be relatively constant over each cycle. In all the cases considered, KC in the range 2.5–17 and U_r in the range 50–70, the instantaneous values of these coefficients do not deviate much from the corresponding mean values. Therefore, the mean coefficients C_D, C_M and C_R can be used to describe adequately the variations of the in-line force coefficient, (38), at every phase. Furthermore, both the mean and instantaneous residual-inertia coefficients C_R and $C_R(t)$ are approximately zero for the range of experiments investigated; thus the third term in the right-hand side of (38) can be neglected. The in-line force coefficient from the present theory as given by (38), can then be simplified to

$$C_F(t) = \frac{F(t)}{\frac{1}{2}\rho U_\infty^2 d} = C_D\left(1 + \frac{r\omega}{U_\infty}\sin\omega t\right)^2 + C_A\frac{\pi}{2}\frac{r\omega^2 d}{U_\infty^2}\cos\omega t,$$

which is found to be identical to Morison's equation written for the present flow.

The semi-empirical Morison's equation was first proposed by Morison *et al.* (1950) for pure oscillatory flow (zero mean) past a stationary cylinder, or an oscillating cylinder in still fluid. Subsequently, it is recommended by the American Petroleum Institute API (1977) that the same equation be valid for superimposed oscillatory
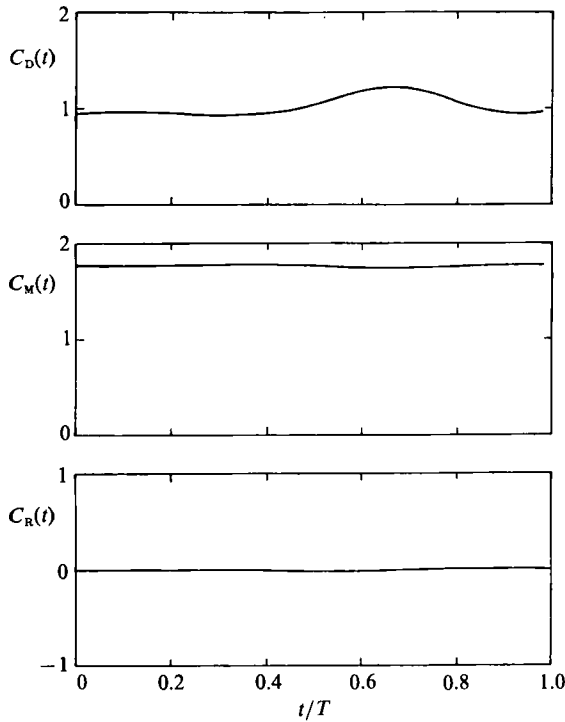
FIGURE 10. An example of computed instantaneous drag, inertia and residual-inertia coefficients during an oscillating cycle. $Re = 27\,000$, $KC = 16.96$, $\beta_t = 393$, $U_r = 68.9$, $VR = 0.25$; $U_\infty = 4.24$ m/s, $r = 0.27$ m, $\omega = 37$ r.p.m.

Author	KC	U_r	VR	C_D
Verley & Moe (1979)	2.5–15	19–46	0.05–0.8	1
Koterayama (1984)	1.3–3.1	24	0.05–0.13	0.95
	5–20	40–60	0.18–0.5	1.1–1.0
Low, Chew & Tan (1989)	2.5–15	20–110	0.05–0.25	1.25–1.0
Present model	2.5–17	50–70	0.05–0.25	1.06–1.01

TABLE 1. Comparison of present and previous results

and mean flow past a stationary cylinder, or an oscillating cylinder in a steady flow. The proposed use of Morison's equation with two constant and independent terms has been subjected to much criticism (Sarpkaya & Issacson 1981) but there is no rigorous alternative available. However, the present potential-flow model which accounts for flow separation has shown that Morison's equation is in some cases a satisfactory model, as the drag and inertia coefficients remain relatively constant and the higher-order term is negligible.

The method can readily be extended to unsteady flow past other symmetrical bodies like a flat-plate, elliptical cylinder whose wetted surfaces can be transformed to the circle in the ζ-plane.

Author	KC	U_r	VR	$C_M(=1+C_A)$
Verley & Moe (1979)	2.5–15	19	0.13–0.8	1.8–1.65
Koterayama (1984)	1.9–2.5	24	0.08–0.1	1.8–1.2
	10–15	40–60	0.16–0.25	1.6
Low, Chew & Tan (1989)	2.5	25–35	0.07–0.13	1.5–1.8
Potential-flow without flow separation	—	—	—	2.0
Present model	2.5–17	50–70	0.05–0.25	1.76

TABLE 2. Comparison of present and previous results

7. Conclusion

A potential-flow wake-source model is developed for steady flow past an in-line oscillating circular cylinder, In the model, the unsteady Bernoulli equation and the conformal transformation are written in a non-inertial frame of reference that is attached to the oscillating cylinder.

The comparison of results as shown in figures 4–6 and 7–8 indicates that the present model gives good predictions of pressure distribution and in-line force variations for an oscillating cylinder in a mean flow.

The in-line force equation obtained from the present model is shown to be comprised of an uncoupled drag term and two inertia terms. The present in-line force agrees in form with Morison's equation except for an additional residual-inertia term that appears in the present formulation. However, the present in-line force equation reduces to Morison's equation when the small residual-inertia term is neglected. This provides some support for the much criticized Morison's equation.

The present modelling enables the calculation of instantaneous drag and inertia coefficients which have not been successfully evaluated in previous attempts. The mean drag and inertia coefficients are also computed. They are shown to compare well with experimental results obtained by previous investigators. The present mean drag coefficients computed are 1.06 and 1.01 for VR of 0.05 and 0.25 respectively. The computed mean inertia coefficients for oscillatory flow are found to remain constant at approximately 1.76.

In the cases considered here, the variations of drag and inertia coefficients over a cycle are shown to be small. This provides support for the use of mean coefficients in Morison's equation, as is commonly done in practice.

REFERENCES

AMERICAN PETROLEUM INSTITUTE (API) 1977 API recommended practice for planning, designing, and constructing fixed offshore platforms. *API RP 2A*. American Petroleum Institute Production Department, 300 Corrigan Tower Building, Dallas, Texas.

ARCHIBALD, R. S. & ROBINS, A. W. 1952 A method for the determination of the time lag in pressure measuring systems incorporating capillaries. *NACA Tech. Note* 2793.

BABA, N. & MIYATA, H. 1987 Higher-order accurate difference solutions of vortex generation from a circular cylinder in an oscillatory flow. *J. Comp Phys.* **69**, 362–396.

BEARMAN, P. W. & FACKRELL, J. E. 1975 Calculation of two-dimensional and axisymmetrical bluff-body potential flow. *J. Fluid Mech.* **72**, 229–241.

CANTWELL, B. & COLES, D. 1983 An experimental study of entrainment and transport in the turbulent near-wake of a circular cylinder. *J. Fluid Mech.* **136**, 321–374.

CELIK, I., PATEL, V. C. & LANDWEBER, L. 1985 Calculation of the mean flow past circular cylinders by viscous-inviscid interaction. *Trans ASME* I: *J. Fluids Engng* **107**, 218–223.

FAGE, A. & JOHANSEN, F. C. 1927 On the flow of air behind an inclined flat plate of infinite span. *Proc. R. Soc. Lond.* A **116**, 170–197.

HURLBUT, S. E., SPAULDING, M. L. & WHITE, F. M. 1982 Numerical solution for laminar two dimensional flow about a cylinder oscillating in a uniform stream. *Trans. ASME* I: *J. Fluids Engng* **104**, 214–222.

JUSTESEN, P. 1991 A numerical study of oscillating flow around a circular cylinder. *J. Fluid Mech.* **222**, 157–196.

KEULEGAN, G. H. & CARPENTER, L. H. 1958 Forces on cylinders and plates in an oscillating fluid. *J. Res. Natl Bureau of Standards* **60**, 423–440.

KIYA, M. & ARIE, M. 1977 An inviscid bluff-body wake model which includes the far-wake displacement effect. *J. Fluid Mech.* **81**, 593–607.

KOTERAYAMA, W. 1984 Waves forces acting on a vertical circular cylinder with a constant forward velocity. *Ocean Engng* **11**, 363–379.

LECOINTE, Y. & PIQUET, J. 1989 Flow structure in the wake of an oscillating cylinder. *Trans. ASME* I: *J. Fluids Engng* **111**, 139–148.

LOW, H. T., CHEW, Y. T. & TAN, K. T. 1989 Fluid forces on a circular cylinder oscillating in line with a uniform flow. *Ocean Engng* **16**, 307–318.

MATTEN, R. B. 1979 Loads on a cylinder in waves, currents and oscillating flow. PhD thesis, Cambridge University Engineering Department.

MILNE-THOMSON, L. M. 1968 *Theoretical Hydrodynamics*, 5th edn (revised). Macmillan.

MORISON, J. R., O'BRIEN, M. P., JOHNSON, J. W. & SCHAAF, S. A. 1950 The forces exerted by surface waves on piles. *Pet. Trans. AIME* **189**, 149–157.

MOSTAFA, S. I. M. 1987 Numerical simulation of unsteady separated flows. PhD thesis, Naval Postgraduate School, Monterey.

PARKINSON, G. V. & JANDALI, T. 1970 A wake-source model for bluff body potential flow. *J. Fluid Mech.* **40**, 577–594.

ROBERTSON, J. M. 1965 *Hydrodynamics in Theory and Application*. Prentice-Hall.

ROSHKO, A. 1954 A new hodograph for free-streamline theory. *NACA Tech. Note* 3168.

SARPKAYA, T. & ISSACSON, M. 1981 *Mechanics of Wave Forces on Offshore Structures*. Van Nostrand Reinhold.

SKOMEDAL, N. G., VADA, T. & SORTLAND, B. 1989 Viscous forces on one and two circular cylinders in planar oscillatory flow. *Appl. Ocean Res.* **11**, 114–134.

SMITH, P. A. & STANSBY, P. K. 1991 Viscous oscillatory flows around cylindrical bodies at low Keulegan–Carpenter numbers using the vortex method. *J. Fluids Struct.* **5**, 339–361.

TAMURA, T., TSUBOI, K. & KUWAHARA, K. 1988 Numerical simulation of unsteady flow patterns around a vibrating cylinder. *AIAA*-88-0128.

WOODS, L. C. 1955 Two-dimensional flow of a compressible fluid past given curved obstacles with infinite wakes. *Proc. R. Soc. Lond.* A 227, 367–386.

WU, T. Y. 1962 A wake model for free-streamline flow theory. *J. Fluid Mech.* **13**, 161–181.

VERLEY, R. L. P. & MOE, G. 1979 The forces on a circular cylinder oscillating in a current. River and Harbour Laboratory, *The Norwegian Institute of Technology, Rep. No.* STF60 A79061.